J. Phys. B: At. Mol. Opt. Phys. **42** (2009) 145202 (10pp) doi:10.1088/0953-4075/42/14/145202

Benchmark differential cross sections for electron impact excitation of the $n = 2$ states in helium at near-ionization-threshold energies

M Hoshino[1], H Kato[1], H Tanaka[1], I Bray[2], D V Fursa[2], S J Buckman[3], O Ingólfsson[4] and M J Brunger[5]

[1] Department of Physics, Sophia University, Chiyoda-ku, Tokyo 102-8554, Japan
[2] Centre for Antimatter-Matter Studies, Curtin University of Technology, GPO Box U1987, Perth, WA 6845, Australia
[3] Centre for Antimatter-Matter Studies, Australian National University, Canberra, ACT 0200, Australia
[4] Department of Chemistry, University of Iceland, Science Institute, Dunkaga 3, Reykjavík 107, Iceland
[5] Centre for Antimatter-Matter Studies, Flinders University, GPO Box 2100, Adelaide, SA 5001, Australia

E-mail: michael.brunger@flinders.edu.au

Received 20 April 2009, in final form 13 May 2009
Published 17 June 2009
Online at stacks.iop.org/JPhysB/42/145202

Abstract
In this paper, we present new normalized experimental differential cross sections for electron impact excitation of the $n = 2$ states in helium. The incident electrons have energies in the range 23.5–35 eV, while the scattered electrons are detected over the angular range 10–130°. Corresponding theoretical results from our convergent close-coupling approach are also presented and in general are in very good accord with our measured data. Where possible, a comparison of the present experimental and theoretical results with those from previous measurements is also made. The case for the $n = 2$ levels in helium constituting a benchmark cross section data set is examined.

1. Introduction

Inelastic cross sections for electron impact excitation of the $n = 2$ (2^3S, 2^1S, 2^3P, 2^1P) levels in helium are scientifically important from both fundamental and applied perspectives, particularly at energies in the range from the first ionization threshold to below about 35 eV. These cross sections dominate the discrete inelastic processes for both the optically allowed 2^1P transition state, as well as in near-threshold excitation for the optically forbidden 2^3P, 2^1S and 2^3S states. From the theoretical perspective, the helium system has also become a standard case for evaluating the validity of collision theory, because a three-electron system in the Coulomb field is fundamental in understanding quantum mechanical collision dynamics. This is particularly true for an appreciation of the exchange interaction and also for typical electron-correlation phenomena. From an applied perspective, knowledge of these cross sections is essential in the design of fusion reactors. This follows as helium is produced as a by-product (usually called 'ash') in the fusion reactor, which can then contribute as one of the important plasma-temperature loss processes in the reactor. On the occasion of the development of the ITER project, it is therefore worthwhile providing a reliable database of helium cross sections so that these effects can be accounted for in its final design.

Since 1990, especially in the low incident energy regime, there have been many high quality measurements focusing on excitation of the $n = 2$ levels. These include data from Brunger *et al* [1], Trajmar *et al* [2], Cartwright *et al* [3], Röder *et al* [4], Allan and colleagues [5, 6] and Lange *et al* [7]. Note that some of these studies only performed measurements at a limited number of energies, while others did not investigate all of the $n = 2$ levels. Further note that some of them were also only relative measurements,

so that while helium is experimentally a comparatively well-studied species for electron collisions, gaps in our knowledge remain. These previous studies can be divided into three characteristic experimental types as follows. In the first four studies, a conventional crossed-beam approach was employed in conjunction with a hemispherical monochromator and hemispherical analyser spectrometer. The scattered electron angular range was between 5 and 130° with an energy resolution of ∼30–40 meV. In the next two most recent methods, from Fribourg University [5, 6], a magnetic angle changer device has additionally been introduced into their tandem hemispherical monochromator and hemispherical analyser spectrometer. In these studies both energy loss and excitation function measurement modes were employed, for the scattering angle range 0–180° and with an energy resolution of ∼20–35 meV. Finally [7], a time-of-flight (TOF) technique was utilized at the Australian National University to analyse the slow scattered electrons that result from near-threshold excitation of the respective $n = 2$ electronic states. This approach followed that developed by Le Clair *et al* [8], but with the significant advantage of being able to access more than one scattering angle (∼40–130° here). As a TOF method it also has the added advantage, at least in principle, of eliminating possible problems associated with the electron optics transmission efficiency in the analyser [1–6].

The present 2^3S (threshold energy = 19.8 eV), 2^1S (threshold energy = 20.6 eV), 2^3P (threshold energy = 20.9 eV) and 2^1P (threshold energy = 21.2 eV) experimental differential cross section (DCS) data are reported for six incident electron energies in the range 23.5–35 eV. The scattered electron angular range was typically 10–130° for these measurements. In our following section we therefore discuss our measurement techniques, while in section 3 details of our convergent close-coupling (CCC) computations are provided. Thereafter a comparison between the results from our new measurements and calculations is made in our section 4, as well as, where possible, a comparison to the results of the previous experiments [1–7]. Finally, some conclusions from the present work are drawn in section 5.

2. Experimental procedures

To measure the inelastic differential cross sections for $n = 2$ electronic state excitation of He, a crossed beam apparatus has been employed. A detailed description on its use and the experimental procedure is found in [9] and will therefore only be briefly summarized here. Electrons produced from an electrostatic hemispherical monochromator intersect with an effusive helium beam at right angles, and the scattered electrons are energy analysed in a second hemispherical analyser. Note that high purity helium was used throughout our measurements. Both the monochromator and the analyser are enclosed in differentially pumped casings, respectively, to reduce the effect of background gases and to minimize any stray electric fields as well as to minimize any electron background. All our electron lens voltages were carefully calculated with an electron trajectory programme. For some lens elements the applied voltages were regulated by programmable power supplies, in order to keep the transmission of the scattered electrons constant. The success of this approach is evident from a comparison between our $n = 2$ DCS at 23.5 eV to that of Lange *et al* [7] (see later). Here very good agreement is found between the present results and that of Lange *et al* [7] whose data, as noted earlier, were taken with a TOF approach where 100% transmission efficiency is guaranteed across the range of scattered electron energies. The overall energy resolution, at Faraday-cup currents of 3–6 nA, was about 30 meV (full width at half-maximum from the observed elastic peaks), more than sufficient to separate the elastic peak from those due to the $n = 2$ electronic-state excitation and to also resolve the individual $n = 2$ levels from one another. This is clearly seen in figure 1, which illustrates some of our typical energy loss spectra, at $\theta = 90°$ in each case, for several of the energies of this study. The incident electron energy is calibrated against the 19.36 eV resonance of He [10]. With respect to the incident electron beam, the scattered electron angular range covered is from 10° to 130°, with an angular resolution of ±1.5°. The cross section normalization method employs a measurement of the ratio of the inelastic to elastically scattered intensity of He under the same experimental conditions, and the use of the known elastic differential cross sections [11] for the particular kinematical conditions under study. Experimental errors [9] are estimated at 15–20%, including components due to the uncertainty in our analyser transmission response, an uncertainty due to errors associated with the elastic normalization cross sections and uncertainties due to any fluctuations in target density and/or incident electron beam current during the measurements. The experimental DCS have been measured at the energies of 23.5, 24, 25, 27.5, 30 and 35 eV for each final electronic state of the $n = 2$ level.

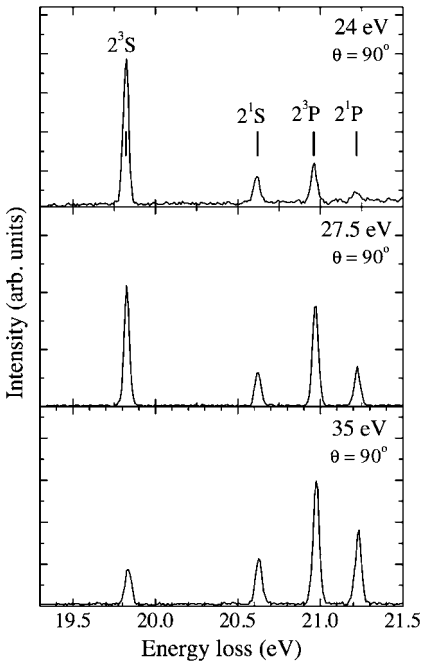

Figure 1. Typical energy loss spectra for the $n = 2$ manifold in helium, at $\theta = 90°$. The respective incident electron energies are 24 eV, 27.5 eV and 35 eV and are denoted in each case in the figure.

Table 1. Present experimental DCS (cm^2 sr^{-1}) for electron impact excitation of the $n = 2$ levels (as labelled) in helium.

Energy (eV)	$\theta(^\circ)$	^{3}S	^{1}S	^{3}P	^{1}P
23.5	60	1.91×10^{-19}	2.57×10^{-20}	5.25×10^{-20}	4.48×10^{-20}
	90	4.41×10^{-19}	8.81×10^{-20}	1.35×10^{-19}	3.83×10^{-20}
24	30	5.78×10^{-20}	1.56×10^{-19}	2.97×10^{-20}	9.05×10^{-20}
	40	7.23×10^{-20}	7.57×10^{-20}	3.62×10^{-20}	9.04×10^{-20}
	50	1.26×10^{-19}	3.51×10^{-20}	5.09×10^{-20}	7.42×10^{-20}
	60	1.76×10^{-19}	1.20×10^{-20}	5.66×10^{-20}	4.51×10^{-20}
	70	2.57×10^{-19}	3.23×10^{-20}	8.45×10^{-20}	4.38×10^{-20}
	80	3.60×10^{-19}	4.93×10^{-20}	9.18×10^{-20}	3.99×10^{-20}
	90	3.90×10^{-19}	9.75×10^{-20}	1.29×10^{-19}	5.69×10^{-20}
	100	4.32×10^{-19}	1.24×10^{-19}	2.06×10^{-19}	5.98×10^{-20}
	110	3.34×10^{-19}	1.56×10^{-19}	2.13×10^{-19}	4.65×10^{-20}
	120	2.09×10^{-19}	1.96×10^{-19}	2.33×10^{-19}	5.21×10^{-20}
	130	1.24×10^{-19}	2.96×10^{-19}	2.97×10^{-19}	4.92×10^{-20}
25.34	10	2.35×10^{-19}	1.12×10^{-18}	5.78×10^{-20}	7.41×10^{-19}
	15	2.12×10^{-19}	9.16×10^{-19}	5.97×10^{-20}	7.19×10^{-19}
	20	1.59×10^{-19}	7.31×10^{-19}	6.92×10^{-20}	6.39×10^{-19}
	30	1.40×10^{-19}	3.32×10^{-19}	8.35×10^{-20}	4.34×10^{-19}
	40	1.15×10^{-19}	9.95×10^{-20}	9.32×10^{-20}	2.40×10^{-19}
	50	1.19×10^{-19}	1.75×10^{-20}	8.81×10^{-20}	1.34×10^{-19}
	55	1.36×10^{-19}	1.62×10^{-20}	9.38×10^{-20}	1.07×10^{-19}
	60	1.61×10^{-19}	1.78×10^{-20}	1.02×10^{-19}	7.77×10^{-20}
	70	1.92×10^{-19}	2.62×10^{-20}	1.07×10^{-19}	6.00×10^{-20}
	80	2.33×10^{-19}	4.57×10^{-20}	1.23×10^{-19}	4.83×10^{-20}
	90	2.29×10^{-19}	6.39×10^{-20}	1.36×10^{-19}	5.21×10^{-20}
	100	1.96×10^{-19}	7.99×10^{-20}	1.57×10^{-19}	4.47×10^{-20}
	110	1.54×10^{-19}	9.97×10^{-20}	1.70×10^{-19}	4.37×10^{-20}
	120	9.77×10^{-20}	1.26×10^{-19}	1.87×10^{-19}	4.15×10^{-20}
	130	5.55×10^{-20}	1.68×10^{-19}	1.99×10^{-19}	3.47×10^{-20}
27.5	10	2.25×10^{-19}	1.29×10^{-18}	1.24×10^{-19}	1.90×10^{-18}
	15	2.29×10^{-19}	1.11×10^{-18}	1.40×10^{-19}	1.85×10^{-18}
	20	2.29×10^{-19}	7.34×10^{-19}	1.34×10^{-19}	1.37×10^{-18}
	30	2.02×10^{-19}	3.14×10^{-19}	1.54×10^{-19}	9.22×10^{-19}
	40	1.70×10^{-19}	8.78×10^{-20}	1.93×10^{-19}	5.11×10^{-19}
	50	1.44×10^{-19}	2.28×10^{-20}	2.03×10^{-19}	2.59×10^{-19}
	60	1.92×10^{-19}	2.15×10^{-20}	2.14×10^{-19}	1.56×10^{-19}
	70	2.41×10^{-19}	4.50×10^{-20}	2.43×10^{-19}	1.13×10^{-19}
	80	3.09×10^{-19}	7.36×10^{-20}	2.72×10^{-19}	1.25×10^{-19}
	90	3.08×10^{-19}	1.05×10^{-19}	2.97×10^{-19}	1.14×10^{-19}
	100	2.34×10^{-19}	1.42×10^{-19}	3.22×10^{-19}	1.05×10^{-19}
	110	2.06×10^{-19}	2.04×10^{-19}	3.76×10^{-19}	1.05×10^{-19}
	120	1.31×10^{-19}	2.78×10^{-19}	3.90×10^{-19}	9.77×10^{-20}
	130	1.19×10^{-19}	3.84×10^{-19}	3.97×10^{-19}	9.45×10^{-20}
30	10	4.49×10^{-19}	1.99×10^{-18}	1.92×10^{-19}	3.86×10^{-18}
	15	4.32×10^{-19}	1.54×10^{-18}	1.83×10^{-19}	3.47×10^{-18}
	20	3.20×10^{-19}	8.92×10^{-19}	1.92×10^{-19}	2.51×10^{-18}
	30	2.18×10^{-19}	2.57×10^{-19}	1.88×10^{-19}	1.20×10^{-18}
	40	1.35×10^{-19}	4.17×10^{-20}	1.89×10^{-19}	5.09×10^{-19}
	45	–	1.67×10^{-20}	–	–
	50	1.15×10^{-19}	7.30×10^{-21}	2.02×10^{-19}	2.47×10^{-19}
	55	–	1.29×10^{-20}	–	–
	60	1.18×10^{-19}	1.95×10^{-20}	2.06×10^{-19}	1.45×10^{-19}
	65	–	2.39×10^{-20}	–	–
	70	1.37×10^{-19}	2.60×10^{-20}	2.08×10^{-19}	1.09×10^{-19}
	75	–	3.26×10^{-20}	–	–
	80	1.64×10^{-19}	4.71×10^{-20}	2.16×10^{-19}	1.03×10^{-19}
	90	1.52×10^{-19}	6.73×10^{-20}	2.27×10^{-19}	9.80×10^{-20}
	100	1.28×10^{-19}	1.04×10^{-19}	2.44×10^{-19}	9.30×10^{-20}
	110	9.76×10^{-20}	1.48×10^{-19}	2.58×10^{-19}	9.13×10^{-20}
	120	7.94×10^{-20}	2.38×10^{-19}	2.87×10^{-19}	8.54×10^{-20}
	130	8.90×10^{-20}	2.88×10^{-19}	2.53×10^{-19}	7.68×10^{-20}

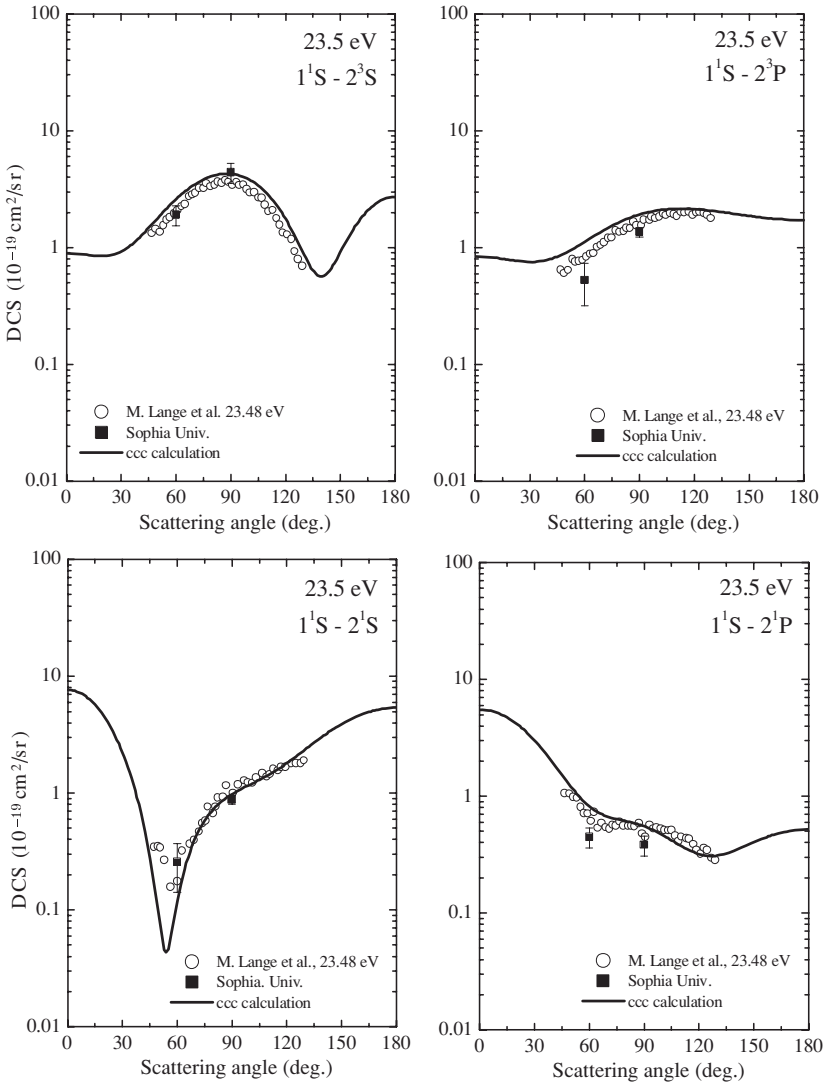

Figure 2. Differential cross sections for 23.5 eV electron impact excitation of the $n = 2$ levels in helium. The present data (■) and CCC calculations (——) are compared against the previous data from Lange *et al* [7] (○).

Table 1. (Continued.)

Energy (eV)	$\theta(^\circ)$	^{3}S	^{1}S	^{3}P	^{1}P
35	10	4.46×10^{-19}	2.10×10^{-18}	1.46×10^{-19}	6.80×10^{-18}
	15	4.00×10^{-19}	1.36×10^{-18}	2.02×10^{-19}	5.47×10^{-18}
	20	3.41×10^{-19}	8.07×10^{-19}	2.03×10^{-19}	3.86×10^{-18}
	30	2.38×10^{-19}	2.00×10^{-19}	2.54×10^{-19}	1.75×10^{-18}
	40	1.67×10^{-19}	2.95×10^{-20}	2.88×10^{-19}	7.30×10^{-19}
	50	9.83×10^{-20}	1.51×10^{-20}	2.99×10^{-19}	3.42×10^{-19}
	60	8.21×10^{-20}	1.07×10^{-20}	3.00×10^{-19}	2.08×10^{-19}
	70	9.42×10^{-20}	3.52×10^{-20}	2.78×10^{-19}	1.80×10^{-19}
	80	9.42×10^{-20}	5.19×10^{-20}	2.43×10^{-19}	1.59×10^{-19}
	90	7.75×10^{-20}	9.74×10^{-20}	2.40×10^{-19}	1.46×10^{-19}
	100	6.57×10^{-20}	1.42×10^{-19}	2.43×10^{-19}	1.31×10^{-19}
	110	5.94×10^{-20}	2.19×10^{-19}	2.42×10^{-19}	1.13×10^{-19}
	120	7.93×10^{-20}	2.49×10^{-19}	2.58×10^{-19}	1.19×10^{-19}
	130	8.62×10^{-20}	3.05×10^{-19}	2.18×10^{-19}	1.13×10^{-19}

3. Theoretical details

The details of the CCC method for electron-helium scattering have been given by Fursa and Bray [12]. Briefly, an orthogonal Laguerre basis is first used to diagonalize the He^+ ion Hamiltonian to obtain negative- and positive-energy one-electron orbitals. These are then used to construct two-electron configurations with one of the orbitals being the He^+

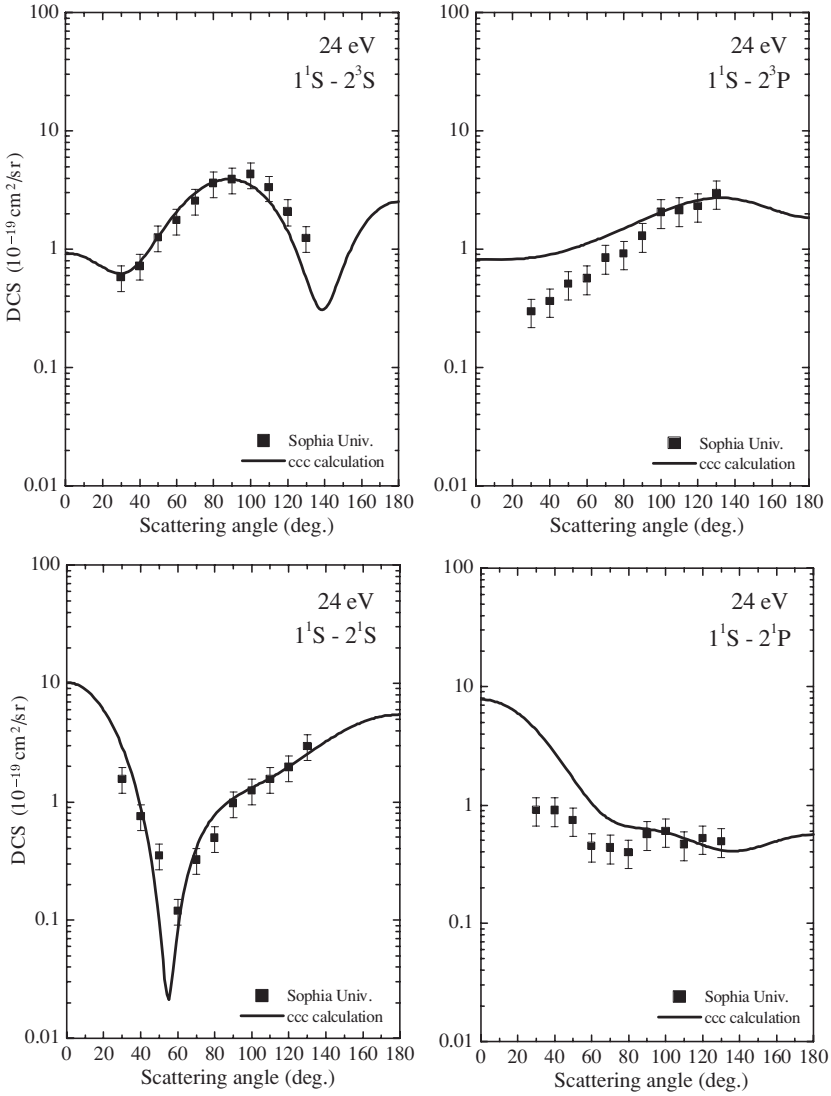

Figure 3. Differential cross sections for 24 eV electron impact excitation of the $n = 2$ levels in helium. The present data (■) and CCC calculations (——) are shown.

1s orbital. This is known as the frozen-core approximation and leads to a reduction of 0.84 eV in the helium ionization energy (24.6 eV). By relaxing the frozen-core approximation we can considerably improve the ionization energy, but at a price of generating many more states for subsequent scattering calculations. Instead, we reduce the incident energy by 0.84 eV and thereby ensure that the total energy in the CCC calculation is the same as in the experiment. As all of the helium discrete excited states are excellent frozen-core states, this approximation is adequate for our purposes.

The helium Hamiltonian is next diagonalized utilizing the constructed two-electron configurations of appropriate symmetry to obtain the helium states to be used in the scattering calculations. By construction, the number of helium states is (almost) twice the number of one-electron orbitals. These states are used to expand the total wavefunction which results in the close-coupling equations. The CCC formulation is in momentum space with the equations taking the form of coupled Lippmann–Schwinger equations. These are solved, after partial wave expansion, typically for the first 10–20 partial waves, with analytical techniques ensuring the treatment of all partial waves when necessary. The solution of the coupled equations leads to the scattering amplitudes that are used to generate data for comparison with experiment.

Convergence in the scattering amplitudes needs to be established against the free parameters of the Laguerre basis. These are the basis size N_l and the exponential fall-off parameter λ_l, for orbital angular momentum $l \leqslant l_{\max}$. Given that presently we are interested in $n = 2$ excited states, setting $l_{\max} = 4$ is sufficient. To make the study of convergence considerably simpler, we set $\lambda_l = \lambda_0$ and $N_l = N_0 - l$. This leaves us to check convergence with just the two parameters N_0 and λ_0.

The rate of convergence for a particular experimental observable is energy dependent. In this work, we present the results over the energy range of 23.5–35 eV. Rather than finding the optimal combination of N_0 and λ_0, at each presented energy, we carried out calculations increasing N_0 from 15 to 20 and varying λ_0 from 1.5 to 2.0 to find a single set of parameters that yields sufficiently convergent results for

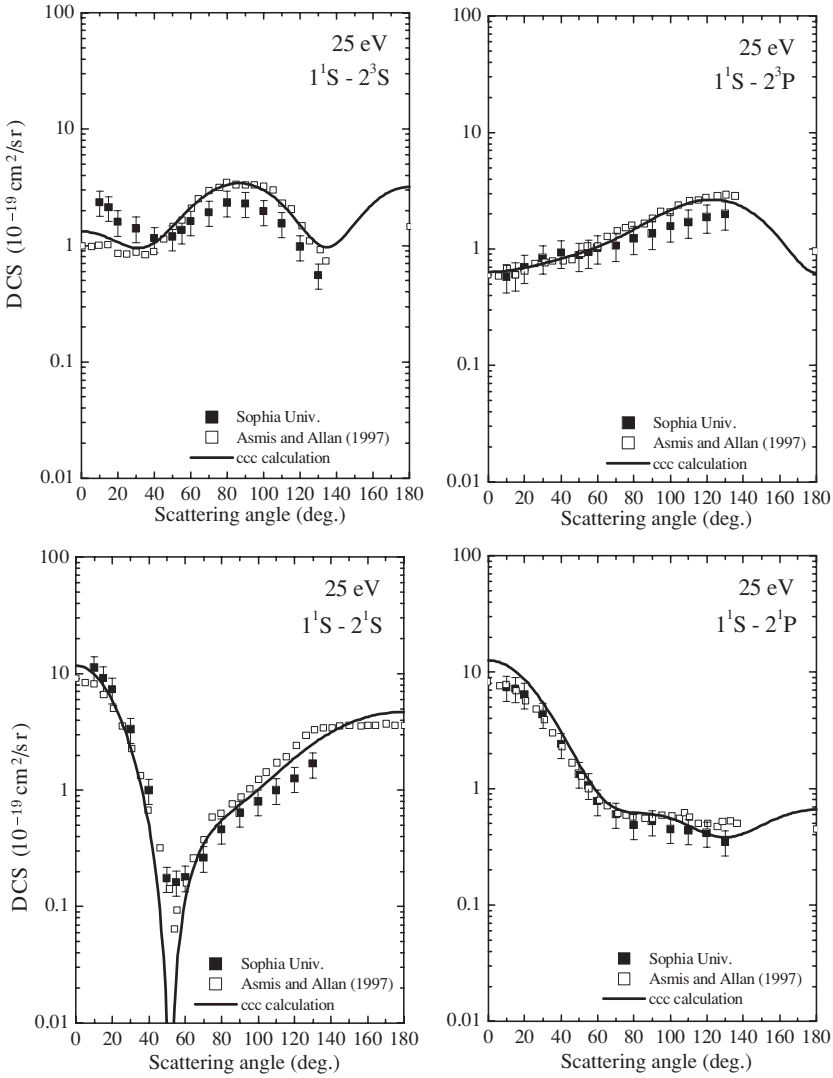

Figure 4. Differential cross sections for 25 eV electron impact excitation of the $n = 2$ levels in helium. The present data (■) and CCC calculations (——) are compared against the previous data from Asmis and Allan [5] (□).

all of the presented cross sections at all of the energies. By taking $N_0 = 20$ and $\lambda_0 = 2.0$ we believe that the presented results are converged to within 5% at most scattering angles, within the frozen-core model.

4. Results and discussion

In table 1 and figures 2–7, we present the results from our current experimental investigation into electron impact excitation of the $n = 2$ levels in helium. Also plotted in figures 2–7 are the results from our corresponding CCC calculations and, where possible, data from previous experimental studies [1, 3–5, 7, 13, 14]. Note that all the error bars plotted in our data in figures 2–7 represent a one standard deviation level estimate of the uncertainty on the present measurements.

Before considering each of figures 2–7 in turn, we begin by making some general observations in regard to the overall behaviour of our measured and calculated DCSs. It is clear from figures 2–7 that the $1^1S \rightarrow 2^1P$ excitation behaves like a classic electric dipole process, in which the parity of the levels change on excitation and there is no change in the spin multiplicity. All the 2^1P angular distributions are forward peaked, with this degree of forward angle peaking in the cross sections increasing as the incident electron energy increases. For the 2^3P state we again have a parity change upon excitation, but here the spin multiplicity changes by 2. This immediately suggests that exchange will be the predominant scattering process, with the angular distributions, which increase monotonically in magnitude with the scattering angle, until around 130° where they then start to again decline in magnitude, being consistent with that population mechanism. For excitation of the 2^1S state there is no change in parity and the spin multiplicity, indicating that direct excitation must be the dominant population mechanism in this case. At all the energies of this study, the respective 2^1S cross sections exhibit a very deep minimum in the scattering angle range 40–60° (see figures 2–7). These minima are seen in both our measurements and CCC calculations, with the experimental depth at each energy being shallower than that correspondingly predicted

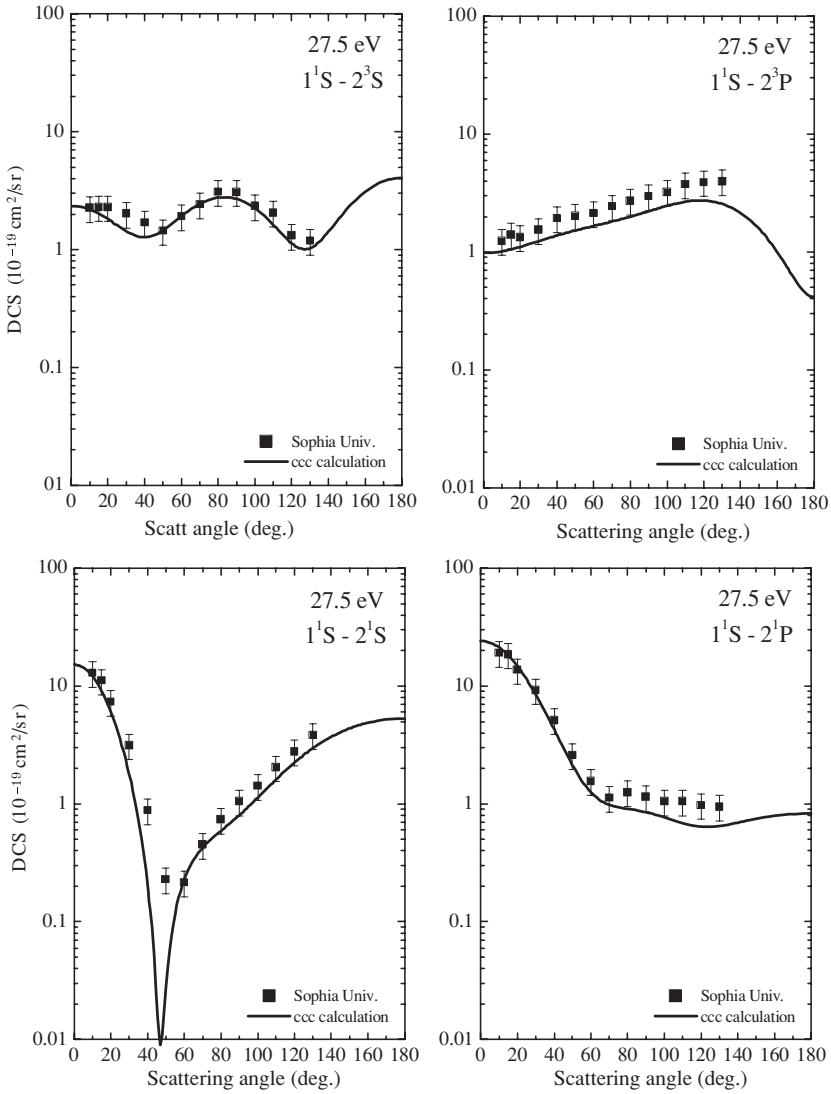

Figure 5. Differential cross sections for 27.5 eV electron impact excitation of the $n = 2$ levels in helium. The present data (■) and CCC calculations (——) are shown.

by our theory. However, this difference is simply understood in terms of the finite angular resolution (1.5° (FWHM)) of our spectrometer. We have theoretically investigated the minimum in the 2^1S cross section, for all the incident electron energies of this work, by considering how this DCS varies with the number of partial waves we include in the calculation. We find that except for the simple case of including just the first partial wave ($\ell = 0$), where the DCS is isotropic, for all other numbers of summed partial waves significant destructive interference occurs in that angular range leading to the observed minimum in the DCS. Finally, for excitation of the 2^3S state, we again have a process where the atomic-state parity does not change but now the spin multiplicity changes by 2. As observed above for the 2^3P state exchange is also expected to play an important role in this scattering process, although the shapes of the 2^3S angular distributions in figures 2–7 additionally suggest important destructive and constructive interference effects between the partial waves. This latter observation was, similar to that for the 2^1S state and again at all of the energies we studied, verified by tracking our CCC partial differential cross sections as a function of summed partial waves in the calculation.

If we now consider figure 2 in more detail, then it is apparent that for each of the $n = 2$ levels there is good agreement between the present DCS (although only for two scattering angles) and the more extensive data from Lange *et al* [7]. This is certainly true to within the combined uncertainties on these two measurements. Agreement between the experimental data and our CCC results is also very good for each state at the incident electron energy of 23.5 eV. At 24 eV (see figure 3), we also find very good agreement between our measured 2^3S and 2^1S DCSs and those from the CCC. This same level of accord is found for excitation of the 2^3P and 2^1P levels for scattering angles between 90 and 130°, but at angles less than 90° the measured data are always somewhat lower in magnitude compared to that predicted by the theory. Overall, however, even here the qualitative trends between our theory and measurement remain consistent. For an incident electron energy of 25 eV, we can in figure 4 also compare the present results to the earlier work of Asmis and Allan

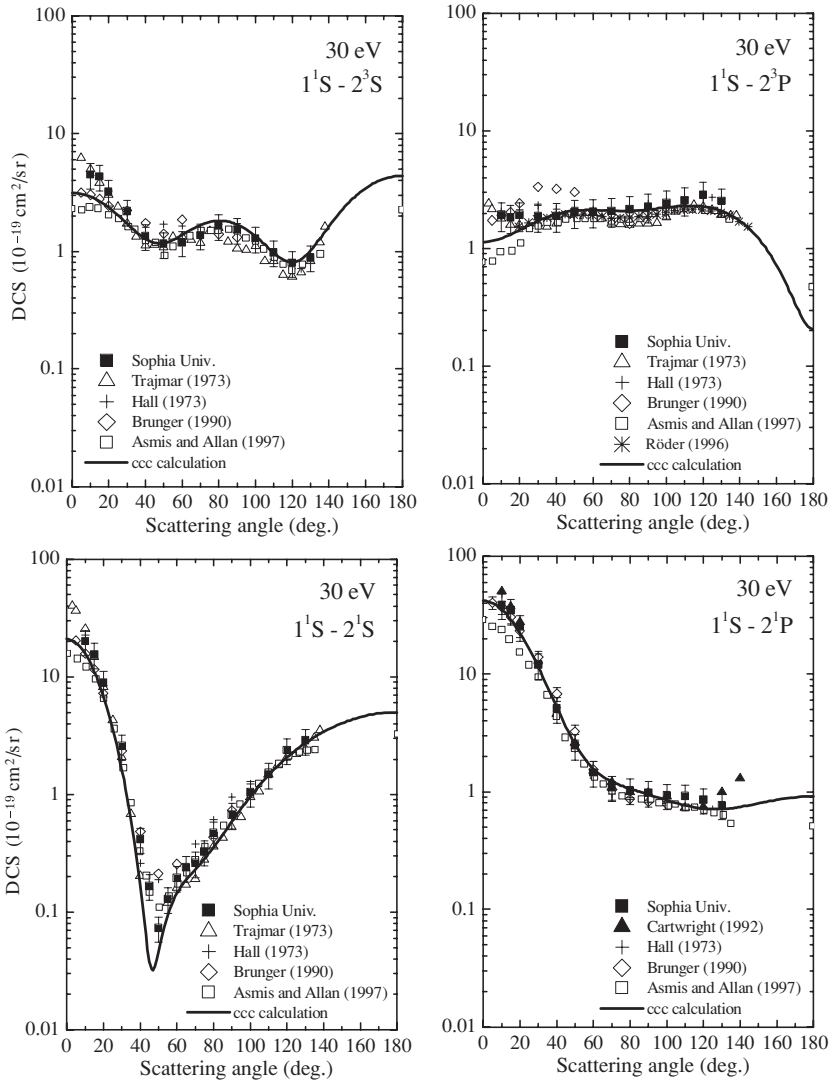

Figure 6. Differential cross sections for 30 eV electron impact excitation of the $n = 2$ levels in helium. The present data (■) and CCC calculations (——) are compared against the previous data from Brunger *et al* [1] (◇), Asmis and Allan [5] (□), Röder *et al* [4] (∗), Hall *et al* [13] (+), Trajmar [14] (△) and Cartwright *et al* [3] (▲).

[5]. If the mutual errors in the two experimental data sets are allowed for, the present data and that of Asmis and Allan are in excellent agreement over the entire common angular range of measurement. The only exception to this general trend is possibly for the 2^3S state at the most forward scattering angles. If we now compare our CCC results to these measured data, then excellent agreement is also found between them for each of the $n = 2$ levels.

In figure 5, we now present the current measured and calculated 2^3S, 2^1S, 2^3P and 2^1P DCSs for an incident energy of 27.5 eV. Just like at 24 eV, this is the first time that such data will have been reported in the literature and as a consequence a comparison with other results is not possible. For each of the $n = 2$ levels the agreement between our measured data and CCC results, from both a qualitative and quantitative perspective, is very good with all the observed angular structure being reproduced in the calculations. There have been significant previous investigations into excitation of the $n = 2$ levels by 30 eV electrons, with a summary of that earlier data [1, 3–5, 7, 13, 14] being plotted in figure 6 along with results from our current measurements and calculations. It is clear from figure 6 that the level of agreement between the previous measurements and the present, when the respective errors are accounted for, is generally excellent. Indeed it is also fair to say that the present CCC results are, for each state, also in excellent accord with the measurements. The major exception to this appears to be at very forward angles for excitation of the 2^3P and 2^1P states, where the cross sections of Asmis and Allan [5] are up to a factor of 3 smaller than the present data and the other measurements [1–4, 13, 14]. In the 2^1P state our CCC calculation strongly supports the present determination of the DCS, but for the 2^3P state it lies between the two groups of data. Therefore, the true nature of the forward angle 2^3P DCS remains somewhat open at this time. Nonetheless, we still have a very strong case for claiming that at 30 eV scattering from the respective $n = 2$ levels is quantitatively understood. Finally, in figure 7, we present original 2^3S, 2^1S, 2^3P and 2^1P DCSs for 35 eV

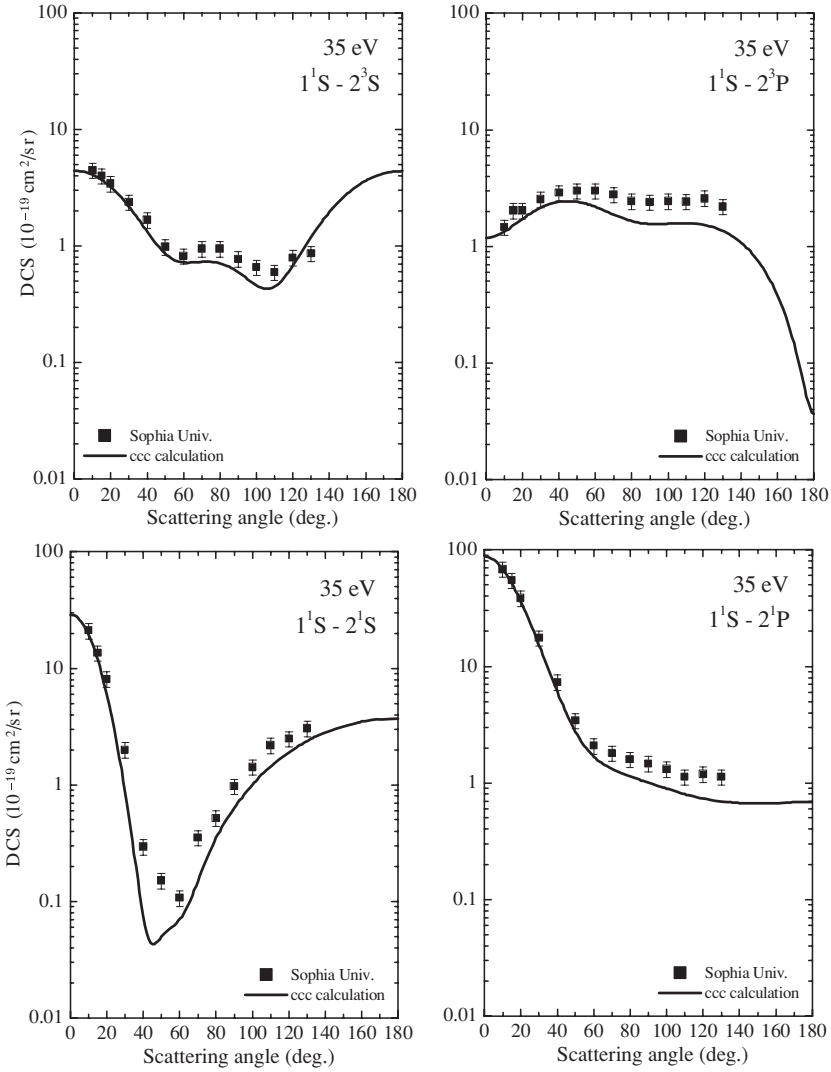

Figure 7. Differential cross sections for 35 eV electron impact excitation of the $n = 2$ levels in helium. The present data (■) and CCC calculations (——) are shown.

electron impact excitation. Consistent with that seen earlier at lower energies, there is again excellent qualitative agreement between our CCC results and our measured data here. The level of quantitative accord between them is additionally very good for each level, with all the angular structure seen in the measurements also being found in the calculations.

The data we have presented in figures 2–7 all support the assertion that the scattering description, for electron impact excitation of each of the $n = 2$ levels in helium, has been benchmarked, at the very least for energies below 35 eV. As it is often hardest to describe near-threshold processes, we believe that the results of our CCC calculations are also very likely to be valid for energies greater than 35 eV [12]. Furthermore, given the very good agreement that we have found between our CCC differential cross section results and all the available experimental DCS data including our own, it follows that the corresponding individual $n = 2$ level CCC integral cross sections (ICS) should also be very accurate. This is very important, as it means that the CCC can be utilized to provide the detailed ICS required for modelling for the effects of ash in, for example, ITER.

5. Conclusions

We have reported new experimental and CCC calculation results of differential cross sections for electron impact excitation of the 2^3S, 2^1S, 2^3P and 2^1P levels in helium, for electrons with incident energies in the range 23.5–35 eV. Agreement between the present measured and calculated DCSs was generally good, often to better than 15%, with both also being in good accord with the available earlier measurements. While some small deviations do remain, the present results confirm that the $n = 2$ excitation in helium is a scattering system that can be considered to have been benchmarked.

Acknowledgments

This work was supported in part by the Australian Research Council through its Centres of Excellence Program. This work was also conducted under the support of the Japanese Ministry of Education, Sport, Culture and Technology. One of us (HK) also acknowledges the Japan Society for the

Promotion of Science (JSPS) for his fellowship as a grant-in-aid for scientific research. We all thank the International Atomic Energy Agency (IAEA) for its support of this work as a part of a data base project. We are grateful for access to the Australian National Computing Infrastructure Facility and its Western Australia node iVEC.

References

[1] Brunger M J, McCarthy I E, Ratnavelu K, Teubner P J O, Weigold A M, Zhou Y and Allen L J 1990 *J. Phys. B: At. Mol. Opt. Phys.* **23** 1325
[2] Trajmar S, Register D F, Cartwright D C and Csanak G 1992 *J. Phys. B: At. Mol. Opt. Phys.* **25** 4889
[3] Cartwright D C, Csanak G, Trajmar S and Register D F 1992 *Phys. Rev.* A **45** 1602
[4] Röder J, Ehrhardt H, Bray I and Fursa D V 1996 *J. Phys. B: At. Mol. Opt. Phys.* **29** L421
[5] Asmis K R and Allan M 1997 *J. Phys. B: At. Mol. Opt. Phys.* **30** 1961
[6] Allan M 2000 *J. Phys. B: At. Mol. Opt. Phys.* **33** L215
[7] Lange M, Matsumoto J, Lower J, Buckman S J, Zatsarinny O, Bartschat K, Bray I and Fursa D V 2006 *J. Phys. B: At. Mol. Opt. Phys.* **39** 4179
[8] Le Clair L R, Trajmar S, Khakoo M A and Nickel J C 1996 *Rev. Sci. Instrum.* **67** 1753
[9] Tanaka H, Ishikawa T, Masai T, Sagara T, Boesten L, Takekawa M, Itikawa Y and Kimura M 1998 *Phys. Rev.* A **57** 1798
[10] Brunt J N H, King G C and Read F H 1977 *J. Phys. B: At. Mol. Phys.* **10** 1289
[11] Boesten L and Tanaka H 1992 *Atom. Data Nucl. Data Tables* **52** 25
[12] Fursa D V and Bray I 1995 *Phys. Rev.* A **52** 1279
[13] Hall R I, Joyez G, Mazeau J, Reinhardt J and Schermann C 1973 *J. Phys.* **34** 827
[14] Trajmar S 1973 *Phys. Rev.* A **8** 191